World Journal of Urology (2025) 43:318
https://doi.org/10.1007/s00345-025-05637-x

RESEARCH

Hydroxycitric acid inhibits ferroptosis and ameliorates benign prostatic hyperplasia by upregulating the Nrf2/GPX4 pathway

Dayong Yang[1] · Chengxi Zhai[1] · Junyu Ren[1] · Jinran Bai[1] · Tao Li[2] · Mingyao Lu[1] · Yongjie Tang[3] · Liangsheng Wei[1] · Rongyao Luo[2] · Fachun Tong[1]

Received: 9 November 2024 / Accepted: 15 April 2025

Abstract

Purpose Benign prostatic hyperplasia (BPH) poses a significant public health challenge, affecting a substantial portion of aging men worldwide. Current therapeutic options offer limited efficacy. The pathogenesis of BPH is multifactorial, involving ferroptosis, oxidative stress, and chronic inflammation. Hydroxycitric acid (HCA) is a natural compound with diverse pharmacological activities, including the inhibition of ferroptosis, anti-inflammatory, anti-oxidative stress, and anti-tumor effects. However, its role in BPH remains unexplored. This study aimed to investigate the effects of HCA on BPH and elucidate the underlying mechanisms, with the goal of providing novel therapeutic insights for BPH treatment.

Methods C57BL/6J mice were used to establish a BPH model induced by testosterone propionate (TP). Animals were then randomly assigned to the following groups: Sham, BPH, BPH + Lip-1, BPH + Bru, BPH + HCA + Bru, and BPH + HCA. Prostate index (PI) was determined, and histopathological changes were evaluated by hematoxylin and eosin (HE) staining. Mitochondrial morphology was analyzed by TEM. The levels of Fe^{2+}, MDA, and GSH in prostate tissues were measured. Western blot analysis was performed to assess the protein expression of Nrf2 and GPX4.Results: Compared to the Sham group, the prostate tissues of the BPH group exhibited typical histopathological features of hyperplasia, including epithelial cell proliferation, increased glandular lumen size. Concurrently, the levels of ferroptosis markers Fe^{2+} ($P < 0.01$) and MDA ($P < 0.001$) were significantly elevated, while the expression of GSH ($P < 0.01$) and GPX4 ($P < 0.05$) was downregulated. Furthermore, mitochondrial morphology showed abnormalities. HCA treatment significantly reduced PI ($P < 0.01$) and attenuated epithelial cell proliferation and glandular lumen enlargement ($P < 0.01$, $P < 0.001$, respectively). HCA also reduced the levels of Fe^{2+} ($P < 0.05$) and MDA ($P < 0.05$), and elevated GSH levels ($P < 0.01$). Furthermore, HCA upregulated the expression of Nrf2 ($P < 0.01$) and GPX4 ($P < 0.01$). The Nrf2 inhibitor Brusatol increased the levels of Fe^{2+} ($P < 0.05$) and MDA ($P < 0.05$), and downregulated the expression of Nrf2 ($P < 0.05$) and GPX4 ($P < 0.05$), thereby attenuating the protective effects of HCA. However, co-administration of HCA and Brusatol partially reversed changes in Fe^{2+} ($P < 0.05$) and MDA ($P < 0.05$) levels, and increased the expression of Nrf2 ($P < 0.05$) and GPX4 ($P < 0.05$), indicating reduction in Brusatol-induced effects. Furthermore, HCA treatment did not significantly affect liver and kidney function markers (AST, ALT, SCR, and UR) ($P > 0.05$).

Conclusion HCA inhibits ferroptosis by activating the Nrf2/GPX4 pathway, thereby ameliorating the pathological changes in BPH induced by TP. This study suggests a novel therapeutic strategy for BPH.

✉ Fachun Tong
13987701922@163.com

[1] Kunming Medical University Sixth Affiliated Hospital (Yuxi People's Hospital), Yuxi City, Yunnan Province, China

[2] Dali University, Dali, Yunnan Province, China

[3] Lincang Mengku Community Health Service Center, Yunnan, China

Published online: 20 May 2025

Graphical abstract

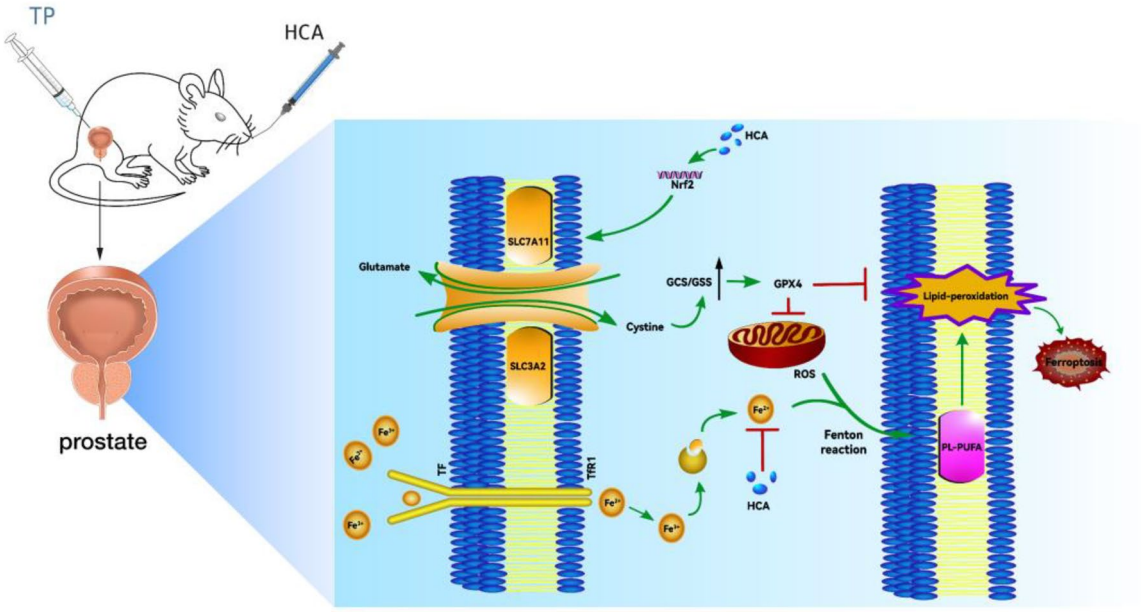

A proposed model elucidates the therapeutic effects of hydroxycitric acid (HCA) on benign prostatic hyperplasia (BPH). On one hand, HCA enhances the transcription of Nrf2, which activates the Xe- system to upregulate the expression ofGPX4, thereby inhibiting ferroptosis. On the other hand, HCA reduces the accumulation of intracellular Fe^{2+}, preventing the Fenton reaction and decreasing the production of lipid peroxides. In summary, HCA improves BPH by inhibiting ferroptosis and modulating iron metabolism.

Keywords Hydroxycitric acid · Benign prostatic hyperplasia · Ferroptosis · Nrf2

Introduction

Benign prostatic hyperplasia (BPH) is the most prevalent non-tumorous hyperplastic condition leading to lower urinary tract symptoms (LUTS), which poses significant health risks to middle-aged and elderly men. Epidemiological studies indicate that the prevalence of BPH rises with age, with figures showing that the prevalence among men over 50 can reach as high as 50% [1, 2]. As the global aging population continues to expand, this proportion may surpass previous estimates, resulting in alarming implications that can severely impact patients' quality of life and impose greater economic burdens on families [3]. BPH typically manifests in a region distinct from that of prostate cancer, predominantly occurring in the transitional zone. Anatomically, BPH is characterized by prostatic enlargement, histologically, the most notable feature is the non-tumorous hyperplasia of epithelial and stromal cells within the periurethral area, which is thought to arise from an imbalance between cell proliferation and apoptosis [4]. Clinically, this pathological hyperplasia often manifests as bladder outlet obstruction and LUTS, with severe cases potentially resulting in chronic renal failure and cardiovascular complications [5]. Currently, the etiology and mechanisms underlying BPH have been extensively studied, identifying numerous factors closely associated with its onset and progression, including hormonal dysregulation [6], stromal-epithelial interactions [7], chronic inflammation [8], autoimmunity [9], oxidative stress [10], and metabolic syndrome [11]. Nonetheless, the precise pathogenesis of BPH remains elusive, and no consensus has yet been achieved.

Alpha-adrenergic blockers (e.g., tamsulosin) and 5-alpha reductase inhibitors (e.g., finasteride and dutasteride) are the primary medications currently used to treat benign prostatic hyperplasia (BPH). These medications work through different mechanisms: alpha-adrenergic blockers selectively inhibit alpha-1 adrenergic receptors in the prostate and bladder neck, reducing the tension in these areas; in contrast, 5-alpha reductase inhibitors function by inhibiting the enzyme 5-alpha reductase, thereby decreasing the conversion of testosterone to dihydrotestosterone (DHT) [12, 13]. Although alpha-adrenergic blockers and 5-alpha reductase inhibitors have been recognized for their efficacy in treating mild BPH, long-term use may be associated with side effects such as erectile dysfunction, retrograde ejaculation, orthostatic hypotension, and gastrointestinal discomfort. Furthermore, discontinuation of these medications often results in symptom recurrence, making long-term

adherence challenging for patients [14–16]. Furthermore, the efficacy of these medications in patients with moderate to severe BPH remains limited. The presence of numerous adverse effects and limitations in the application of these medications has hindered their widespread adoption and use. Therefore, elucidating novel pathophysiological mechanisms underlying BPH is crucial for the development of safer, more effective alternative therapies with fewer side effects that are suitable for long-term use.

Ferroptosis is a newly discovered form of cell death, which significantly differs from traditional modes of cell death such as apoptosis, autophagy, and necrosis. It is characterized by excessive oxidative damage to cellular membrane lipids during the cell death process, resulting in the accumulation of lipid peroxides that exceed the clearance capacity of the body's antioxidant systems, ultimately leading to ferroptosis. This process is typically triggered and regulated by various factors, including redox homeostasis, antioxidant genes, iron ions, energy metabolism, and lipid metabolism [17, 18], all of which collectively facilitate the ferroptosis process. Nuclear factor erythroid 2-related factor 2 (Nrf2), an antioxidant transcription factor, regulates the transcription of various antioxidant and ferroptosis-related enzymes, including glutathione peroxidase 4 (GPX4), which plays a critical role in the removal of lipid peroxide accumulation [19–23]. Research indicates that ferroptosis is involved in the progression of various pathological conditions, including malignant tumors [23, 24], neurodegenerative diseases [25, 26], and ischemia–reperfusion injury [27, 28]. Furthermore, an increasing number of studies suggest that ferroptosis also plays a regulatory role in physiological processes such as embryonic development and tissue homeostasis [18]. Recent studies have demonstrated that ferroptosis plays a key role in benign prostatic hyperplasia (BPH). For instance, research by Li [29] found that in BPH tissues, there were not only low levels of apoptosis but also elevated levels of ferroptosis and autophagy. Zhou [30] transcriptomic and non-targeted metabolomic analyses suggested that ferroptosis may play a critical role in BPH, identifying CBR3-AS1-has-miR-5p-MAP3K5 as one of the competitive endogenous RNA (ceRNA) networks involved in ferroptosis during the progression of BPH, potentially providing a novel therapeutic target for treating BPH. Additionally, Zhan [31] RNA sequencing results showed that taurine upregulated gene 1 (TUG1) was significantly associated with prostate volume and the degree of inflammatory infiltration in BPH patients. They discovered that TUG1 promotes the expression of GPX4 by competitively binding with miR-188-3p, thereby influencing ferroptosis. These findings open new avenues for elucidating the pathogenesis of BPH and identifying novel therapeutic targets, potentially establishing crucial targets for the treatment of BPH in humans.

Hydroxycitric acid (HCA), the main active component of Garcinia mangosteen extract, possesses a wide range of pharmacological activities, including antitumor, antioxidative stress resistance, and anti-inflammatory properties [32–34]. Recent studies have also shown that HCA can mitigate organ ischemia–reperfusion injury by inhibiting ferroptosis [35]. However, the therapeutic efficacy and potential mechanisms of HCA in treating benign prostatic hyperplasia (BPH) have not been fully reported, while ferroptosis is considered one of the important mechanisms involved in the progression of BPH. Therefore, we hypothesize that HCA may improve BPH by inhibiting ferroptosis and will explore the potential mechanisms of HCA in BPH, aiming to provide a new reference for the treatment of BPH.

Materials and methods

Reagents and antibodies

Testosterone propionate (TP) was obtained from Jingke Biochemical Products Co., Ltd. (Sichuan, China). Injectable penicillin G potassium was purchased from Keda Animal Pharmaceutical Co., Ltd. (Jiangxi, China). HCA was procured from QuanAo Biotechnology Co., Ltd. (Xi'an, China). A colorimetric iron content detection kit was obtained from Tongren Chemical Co. (Kyushu, Japan). A microplate reduction-type glutathione (GSH) assay kit was acquired from Nanjing Jiancheng Bioengineering Institute (Nanjing, China). A proteinase inhibitor cocktail and ECL detection reagents were obtained from Proteintech (Wuhan, China). RIPA lysis buffer and BCA assay kits were purchased from Yamei Biotechnology (Shanghai, China). Hematoxylin and eosin (H&E) staining kits and a malondialdehyde (MDA) lipid oxidation detection kit were acquired from Biyuntian Biotechnology (Shanghai, China). Liproxstatin-1, brusatol, DMSO, PEG 300, and Tween 80 were purchased from MCE (New Jersey, USA).

The following antibodies were used for the detection of relevant proteins: Nrf2 (Catalog No. 12721 T, CST), GPX4 (Catalog No. ab20777, Abcam), and goat anti-rabbit/mouse secondary antibodies (Catalog No. S0001/S0002, Affinity Biosciences).

Animal experiments

Construction of Castration and Sham Surgery Models: Prior to the experimental procedures, mice underwent either castration or sham surgery. One hour post-surgery, the mice

were monitored for respiratory distress, signs of scrotal swelling, and any hemorrhage at the incision site. For all mice subjected to either castration or sham surgery, penicillin G potassium (250,000 units/kg/day) was administered intramuscularly in the thigh for three consecutive days to prevent surgical site infections. The mice were then observed for a period of seven days. The specific procedures for castration and sham surgery are as follows:

Castration Surgery: Briefly, after induction of anesthesia with 5% isoflurane for five minutes, the mice were placed in a supine position on a surgical table. Scrotal hair was shaved to expose the surgical area, and standard disinfection procedures were performed. A longitudinal incision of approximately 1 cm was made in the midline of the scrotum. The tissues were dissected layer-by-layer until the testes were reached. The tunica was incised to expose both testes, which were subsequently excised. The remaining tissue was sutured with 5–0 surgical silk. After confirming that there was no significant bleeding, the tunica and skin were sutured in layers using 5–0 silk, followed by a second disinfection of the surgical area.

Sham Surgery: The procedure followed similar steps, with layer-by-layer dissection until both testes were reached, without excision. Subsequently, the tunica and skin were sutured in layers using 5–0 surgical silk, and the surgical area was disinfected once more.

Drug preparation

Preparation of Liproxstatin-1 Working Solution: Liproxstatin-1 is an effective ferroptosis inhibitor. The preparation will strictly follow the instructions provided in the product manual and the recommended in vivo concentrations. A specific mass of Liproxstatin-1 will be weighed and dissolved in DMSO to prepare a stock solution of 25.0 mg/ml, which will be aliquoted and stored at – 20 °C for future use.The calculation of the specific dosing regimen is as follows: The actual body weight of the mice will be measured, and the working solution will be prepared according to the recommended solubilization scheme in the product manual: 10% DMSO (from the stock solution) → 40% PEG300 → 5% Tween-80 → 45% sodium chloride. The required volumes of the solubilizing agents will be calculated, and the solutions will be added sequentially, mixed well, and prepared as a working solution of Liproxstatin-1 (2.5 mg/ml) for use.

Preparation of Brusatol Working Solution: Brusatol is a unique inhibitor of the Nrf2 signaling pathway, capable of suppressing intracellular Nrf2 transcriptional activity. The preparation will strictly follow the instructions provided in the product manual and the recommended in vivo concentrations. A specific mass of Brusatol will be weighed and dissolved in DMSO to prepare a stock solution of 25.0 mg/ml, which will be aliquoted and stored at – 20 °C for future use.The calculation of the specific dosing regimen is as follows: The actual body weight of the mice will be measured, and the working solution will be prepared according to the recommended solubilization scheme in the product manual: 10% DMSO (from the stock solution) → 40% PEG300 → 5% Tween-80 → 45% sodium chloride. The required volumes of the solubilizing agents will be calculated, and the solutions will be added sequentially, mixed well, and prepared as a working solution of Brusatol (2.5 mg/ml) for use.

Preparation of HCA Working Solution:The dosing of HCA is determined by converting the human dosage to the mouse model equivalence as a reference [36, 37], with the final oral gavage dose for mice determined to be 4 g/kg/day. A specific mass of HCA will be weighed and diluted in saline to prepare a working solution with a final concentration of 2 g/ml for future use.

Preparation of Testosterone Propionate (TP) Working Solution: After weighing, a syringe will be used to withdraw the testosterone propionate solution according to the dosing regimen of 5 mg/kg/day for future use.

Preparation of Saline Working Solution:After weighing, an equal volume of saline solution will be withdrawn using a syringe, following the administration method used for testosterone propionate, for future use.

Animal studies

Male C57BL/6 J mice, aged 6–8 weeks and weighing between 20 and 25 g, were obtained from the Kunming Medical University Experimental Animal Center. The mice were housed in a controlled environment with a temperature of 23.0 ± 2 °C, humidity of 50 ± 10%, and a light–dark cycle of 12 h. During the experimental period, all mice had ad libitum access to standard chow and drinking water. All experimental procedures involving animals were conducted in strict accordance with the Guidelines for the Care and Use of Laboratory Animals published by the National Institutes of Health (NIH). At the conclusion of the experiment, euthanasia was performed on all mice via inhalation of excessive carbon dioxide to minimize suffering.

Figure 1 illustrates the experimental workflow. After weighing, the experimental mice underwent either castration or sham surgery and were randomly divided into six groups: Sham, BPH, BPH + Lip-1, BPH + Bru, BPH + HCA + Bru, and BPH + HCA, with eight mice in each group. Except for the Sham group, which received intraperitoneal injections of physiological saline, the remaining five groups were administered daily intraperitoneal injections of 5 mg/kg testosterone propionate. The working solution of Liproxstatin-1 (Lip-1) was injected intraperitoneally 30 min prior to each use, while the working solution of Brusatol (Bru) was administered intraperitoneally 48 h before the

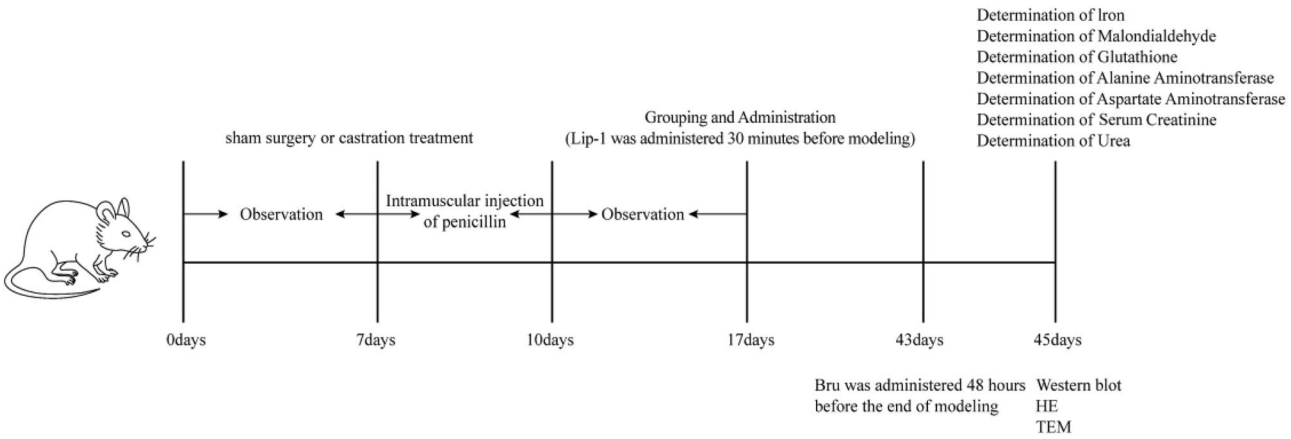

Fig. 1 illustrates a schematic diagram of the experimental procedure. The BPH model was induced by the injection of testosterone propionate. On day 7, sham surgery and castration were performed; on day 17, grouping was conducted followed by administration of Lip-I and HCA; on day 43, intraperitoneal injection of Bru was carried out; and on day 45, modeling was completed and experiments were conducted (including measurements of iron content, MDA, GSH, AST, ALT, CREA, UREA, as well as HE staining, WB, and TEM). *BPH* Benign Prostatic Hyperplasia; *Lip- I* Liproxstatin-1; *HCA* Hydroxycitric Acid; *MDA* Malondialdehyde; *GSH* Glutathione; *ALT* Alanine Aminotransferase; *AST* Aspartate Aminotransferase; *CREA* Serum Creatinine; *UREA* Urea Nitrogen; *HE* Hematoxylin and Eosin Staining; *TEM* Transmission Electron Microscopy

conclusion of the modeling phase. The HCA working solution was provided via gavage. The dosages of all substances were adjusted based on the daily weight measurements of the animals; all treatments, apart from Bru, continued for a duration of 4 weeks. Finally, to comprehensively assess the long-term effects of HCA on the liver and kidneys, we continued administering HCA (4 g/kg/d) by gavage once daily for one year following the completion of the 28-day modeling period.

Collection and processing of prostate tissue and serum samples

Following the final treatment, all animals were fasted for 6–8 h. Once anesthesia was induced using 5% isoflurane, cardiac blood collection was performed, followed by the rapid excision of prostate tissue, which was subsequently washed with pre-chilled 1.15% KCl solution. After washing, the prostate tissue was dried and weighed, and the body weight of the mice was recorded to calculate the Prostate Index (PI). A portion of the prostate tissue was fixed in 4% paraformaldehyde and 2.5% glutaraldehyde for histological analysis, while the remaining tissue was stored at – 80 °C for biochemical analysis. The Prostate Index is an indicator used to evaluate the relative weight of prostate tissue in relation to the body weight of mice. This index is instrumental in studying the physiological and pathological changes in the prostate and serves as a critical marker of prostate health and function. The formula for its calculation is as follows:

$$\text{Prostate Index (PI)} = \text{Prostate Weight (mg)} / \text{Body Weight (g)} \times 100\%$$

Blood samples were collected using the cardiac puncture method and allowed to stand at 4 °C for 2 h before centrifugation at 3000 g for 10 min at 4 °C to obtain serum. The extracted serum was aliquoted and stored at – 80 °C for subsequent liver and kidney function assays.

Hematoxylin and eosin (HE) staining of prostate tissu

The ventral prostate tissue was fixed in 10% formalin for 24 h, followed by dehydration through a gradient of ethanol, paraffin embedding, and xylene clearing. Sections were cut to a thickness of 4 μm, then placed on slides at 45 °C and dried at 60 °C, followed by a de-waxing procedure. After hydration, standard HE staining was performed, followed by dehydration through a gradient of ethanol, clearing with xylene, and mounting with neutral resin. Images were acquired using a fluorescence microscope (Zeiss, Axioscope 5, Germany), and ImageJ software (NIH, USA) was utilized to quantify the epithelial cell membrane thickness and lumen area. The thickness of the epithelial cell membranes and lumen areas were calculated for each group.

Transmission electron microscopy (TEM)

Fresh prostate tissue was cut into cuboids measuring 1 mm × 1 mm × 3 mm and fixed with 2.5% glutaraldehyde (P1126, Solarbio) at 4 °C for 1–1.5 h. The samples were then transferred to 1% osmium tetroxide (OsO4) and fixed at 4 °C for an additional 2 h. Following this, a series of ethanol dehydrations and a 5-min transition in acetone were

performed before embedding the samples in epoxy resin and double staining with 2% uranyl acetate and 1% lead citrate. Once the samples were dried, transmission electron microscopy (JEM-1400Plus, Japan) was used to observe the ultrastructure of the tissue mitochondria to determine the occurrence and severity of ferroptosis.

Measurement of iron content

To determine iron levels, we strictly followed the protocol provided by the colorimetric iron assay kit, adding 4 to 10 times the volume of Assay Buffer to the collected supernatant for later use. Assay Buffer and Reducer solution were added to the sample tubes separately and incubated at 37 °C for 15 min. Then, 105 µl of each solution was transferred to a 96-well plate, to which 100 µl of substrate working solution was added and incubated at 37 °C for 1 h. The absorbance was measured at 593 nm using a microplate reader.

Measurement of malondialdehyde (MDA) levels

We performed the measurement of MDA levels in prostate tissue following the instructions provided in the lipid peroxidation (MDA) detection kit. Briefly, a 10% prostate tissue homogenate was prepared in PBS on ice and then centrifuged (12,000 g, 10 min, 4 °C). Following the instructions, MDA working solution was added, mixed thoroughly, and then heated at 100 °C for 15 min before cooling in a water bath to room temperature. The mixture was then centrifuged again (1000 g, 10 min) to obtain the supernatant, and the MDA levels were measured by assessing the absorbance at 532 nm.

Determination of GSH levels

We measured the levels of reduced glutathione (GSH) in the prostate tissue following the instructions of the microplate GSH assay kit. In brief, a precise amount of approximately 0.02 g of tissue was weighed and mixed with reagent 1 to prepare a 10% homogenate of prostate tissue. The homogenate was then centrifuged (3500 g, 10 min, 4 °C), and the supernatant was added separately to the coloring reagent and buffer solution. After mixing, the solution was allowed to sit for 5 min. The relative content of glutathione was determined by measuring the absorbance at 405 nm.

Assessment of liver and kidney function

To assess the potential damage of the drug to the liver and kidneys, we entrusted the Clinical Laboratory of Yuxi People's Hospital to evaluate liver and kidney function parameters (AST, ALT, SCR, and UR) in serum samples.

Western blotting

Briefly, 0.5 ml of RIPA lysis buffer was used to prepare a tissue lysate from the mouse prostate, along with the addition of 0.1 ml of proteinase inhibitor mixture for mechanical homogenization. The mixture was lysed on ice for 30 min and then centrifuged (20,000 g, 10 min, 4 °C) to remove insoluble material. The supernatant was collected as the nuclear protein fraction, and protein concentration was determined using a BCA assay kit. Equal amounts of the sample were subjected to electrophoresis and transferred to a PVDF membrane, which was then blocked at room temperature for 2 h with 5% fat-free milk. After washing, GPX4 antibody (1:1000, ab20777, Abcam, USA) and NRF2 antibody (1:1000, 12721 T, Cell Signaling Technology, USA) were added and incubated overnight on a shaker at 4 °C. After washing, goat anti-rabbit/mouse secondary antibody (1:10,000, S0001/S0002, Affinity Biosciences, Jiangsu, China) was added and incubated at room temperature for 2 h. The immunoreactive bands were visualized using ECL chemiluminescent reagents, and the chemiluminescent signals were detected using a fully automated gel imaging analysis system (iBright CL1500, Thermo Fisher Scientific, USA). Quantification of the bands was performed using ImageJ software (NIH, USA).

Statistical analysis

In this study, all data are presented as mean ± standard deviation (M ± SD) and statistical analyses were performed using GraphPad Prism software (v10.1.2, GraphPad Software). To determine intergroup differences, we first applied the Shapiro–Wilk test to evaluate the normality of data distribution, followed by Student's t-test to compare means between two groups. Additionally, one-way ANOVA and Dunnett's post-hoc test were used for multiple comparisons. All experiments were performed at least in triplicate. Differences were considered statistically significant when $P < 0.05$.

Results

Ferroptosis as a pathological feature of the BPH animal model

To further confirm that ferroptosis may be one of the pathological mechanisms in benign prostatic hyperplasia (BPH), we first analyzed prostate tissue from TP-induced BPH mice. Histological examination using hematoxylin and eosin (HE) staining revealed disorganized arrangement of epithelial cells, irregular duct and acinar morphology, and varying degrees of increased epithelial thickness, characterized by papillary or

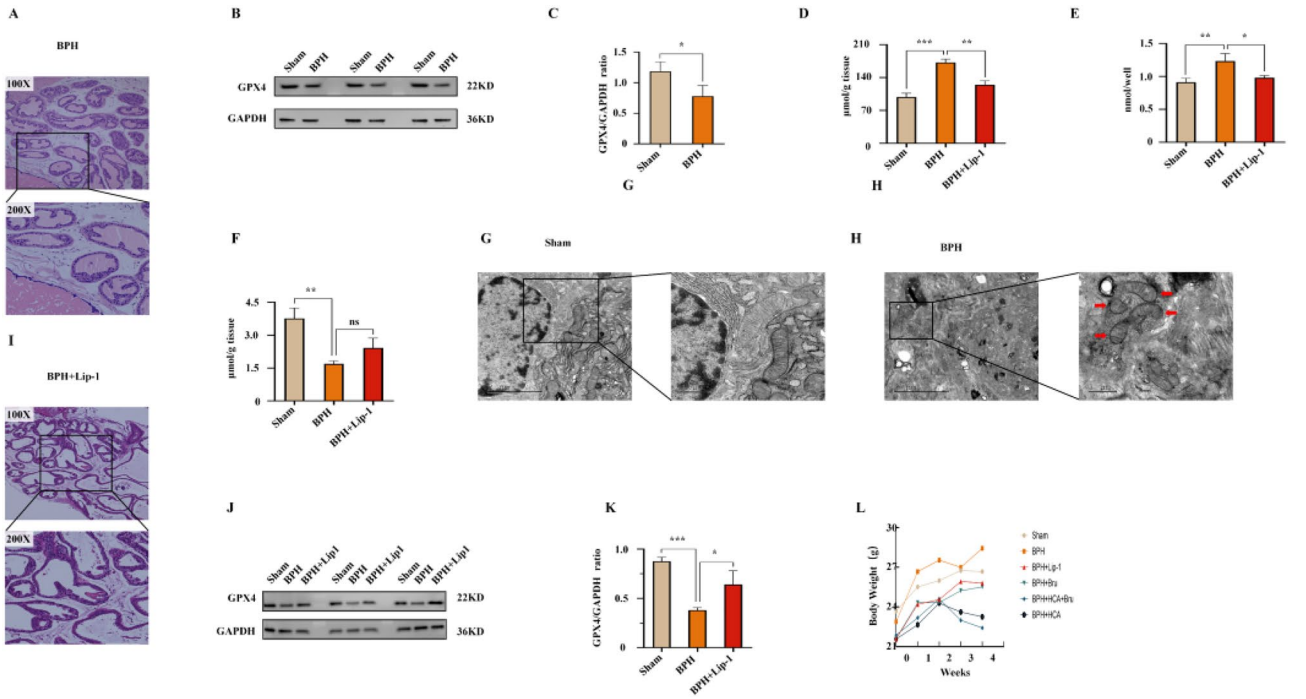

Fig. 2 Ferroptosis is involved in prostatic hyperplasia and can be reversed by ferroptosis inhibitors. **A** HE Staining Results of the BPH Group. **B**-**C** Expression levels ofGPX4 protein in prostatic hyperplasia. **D**-**F** The levels of MDA, Fe^{2+} and GSH in the prostate homogenates of different groups of mice. **G**-**H** Representative TEM images of mitochondria in prostate tissue observed by transmission electron microscopy (scale bars: 2 μm and I μm). **I** HE Staining Results of the BPH + Lip Group. **J**-**K** Changes in GPX4 protein levels in prostate tissue following Lip-I treatment. **L** XY plot of mouse weight changes. Data are presented as mean ± standard deviation (M ± SD). Comparisons with the Sham group **p < 0.0I, ***p < 0.00 I. comparisons with the BPH group *P < 0.05, **p < 0.01, ns > 0.05

villous projections into the lumen, resulting in a proliferative folding appearance (Fig. 2A). These findings are consistent with the pathological features of BPH, indicating successful model establishment. Subsequently, we evaluated the expression of GPX4 using Western blotting, which showed a significantly decreased level of GPX4 compared to the normal control group (Fig. 2B). GPX4 is widely recognized as a marker for ferroptosis, and its expression level is negatively correlated with ferroptosis. Based on these findings, we collected prostate tissue from the TP-induced BPH mouse model for further experiments.

Iron accumulation, lipid peroxidation, and reduced GPX4 are established markers of ferroptosis [18, 38]. We then assessed the levels of lipid peroxidation, iron content, and GSH levels in prostate tissue. Compared to the Sham group, the TP-induced BPH group exhibited significantly elevated levels of malondialdehyde MDA and iron (Fig. 2D, E), while GSH synthesis was significantly reduced (Fig. 2F). Importantly, transmission electron microscopy (TEM) analysis of the mitochondrial morphology in the prostate epithelial cells of the BPH group revealed structural changes such as mitochondrial shrinkage and reduced cristae compared to the Sham group, which are noteworthy alterations associated with BPH (Fig. 2G, H). To further confirm the occurrence of ferroptosis, we administered Lip-1 (a ferroptosis inhibitor) intraperitoneally thirty minutes prior to TP injection. As expected, administration of Lip-1 reduced MDA levels (Fig. 2D) and successfully reversed iron overload (Fig. 2E), although its impact on GSH levels was not significant (Fig. 2F). Furthermore, HE staining indicated an improvement in prostatic hyperplasia (Fig. 2I). Western blot analysis further confirmed the upregulation of the key ferroptosis protein GPX4 (Figs. 2J, K). Overall, these results suggest that ferroptosis is involved in the pathogenesis and progression of BPH and can be reversed by ferroptosis inhibitors.

The effect of HCA on the phenotypic characteristics of a BPH animal model

Compared to the control group, the TP-induced BPH group exhibited a significant increase in prostate relative weight. Given that the prostate index (PI) is one of the indicators for assessing the therapeutic efficacy of prostatic hyperplasia, we calculated the PI for each group at the end of

Table 1 Body weight, prostate weight, and prostate index in mice

groups	weight			Prostate	Prostate index (PI)
	Start (g)	finally (g)	weight gain (g)	Mass (mg)	
Sham	23.69±0.8709	26.68±1.536	2.988±1.383 *	25.50±4.536	1.015±0.1303***
BPH	22.89±1.467	28.43±1.595	5.538±2.029	37.75±5.751	1.411±0.2505
BPH+Lip-1	21.59±1.352	25.81±1.068	4.225±0.796 ns	21.88±3.044	0.9484±0.1047 ####
BPH+Bru	21.61±0.7736	25.51±2.192	3.9±2.61 ns	38.88±7.240	1.579±0.2449 ns
BPH+HCA+Bru	21.88±0.6065	22.41±1.655	0.5375±1.897 ####	20.75±3.240	0.9179±0.1829 ####
BPH+HCA	21.58±0.6159	23.25±1.09	1.675±1.125 ###	20.50±3.117	0.9178±0.1547 ####

Data are expressed as mean ± standard deviation (M ± SD) (n = 8 per group). Compared to Sham group **P < 0.05 and ***P < 0.001; compared to the BPH group ###P < 0.001, and ####P < 0.0001

the experiment (Table 1). The PI of the BPH group was significantly increased compared to the Sham group. In comparison to the BPH group, both the BPH + HCA and BPH + Lip-1 groups exhibited a significant reduction in PI, while the BPH + Bru group showed no significant change. The PI of the BPH + HCA + Bru group was significantly reduced compared to the BPH + Bru group. Notably, in mice subjected to HCA intervention, we observed a decrease in appetite and overall body weight, which may be attributed to the competitive inhibition of ATP-citrate lyase activity [39].

The effect of HCA intervention on HE staining in the BPH animal model

Following 28 days of modeling and drug administration, prostate morphology was observed, revealing a significant increase in prostate volume in both the BPH and BPH + Bru groups. In contrast, after treatment with HCA and the ferroptosis inhibitor (Lip-1), the prostate volumes in both groups markedly decreased when compared to the BPH group. with a notable reduction in the BPH + HCA + Bru group compared to the BPH + Bru group. To further observe and evaluate histological changes in the prostate, we performed HE staining analysis on prostate tissues from each group, as shown in the results (Fig. 3A).In the Sham group, the structure of prostate epithelial cells was intact and well-defined, arranged in a single layer with a regular glandular lumen shape, and pink secretions were present within the lumen. The BPH group exhibited a notable increase in gland number, with disordered arrangement of epithelial cells, irregular shapes of ducts and acini, and varying degrees of hypertrophy of glandular epithelial cells. Some cells extended into the lumen in a papillary or villous manner, leading to infolding within the lumen. Occasional retention of pink secretions was noted, and there was significant stroma hyperplasia, consistent with the histopathological characteristics of BPH, confirming the successful establishment of the BPH model. After treatment with the ferroptosis inhibitor (Lip-1), the HE staining results in the BPH + Lip-1 group indicated a significant reduction in the degree of papillary hyperplasia of epithelial cells compared to the BPH group, alongside notable decreases in cell thickness and marked increases in lumen area. Following treatment with HCA and Bru, the HE staining results indicated that the lumen area of prostate epithelial cells in the BPH + Bru group significantly decreased compared to the BPH group, while there was no noticeable change in thickness. Conversely, the BPH + HCA group demonstrated a significant reduction in epithelial cell thickness and a substantial increase in lumen area, with clear and intact glandular lumen shapes and tightly organized cells, nearly restoring a normal prostate tissue structure. In comparison to the BPH + Bru group, the BPH + HCA + Bru group showed significant reductions in epithelial cell thickness and substantial increases in lumen area. The HE results across all groups indicated that the improvement in the BPH + HCA group was particularly pronounced. Finally, the thickness of epithelial cells and lumen area were quantified using ImageJ software, which further corroborated the results (Fig. 3B, C).

HCA improves the BPH animal model by inhibiting ferroptosis through the activation of the Nrf2/GPX4 pathway

Our results have shown that ferroptosis is one of the mechanisms involved in BPH. Combined with recent reports by Lu [35]. indicating that HCA inhibits ferroptosis, and supported by HE results confirming the improvement of BPH by HCA, we hypothesize that the beneficial effects of HCA on BPH are mediated through its impact on ferroptosis. To validate this hypothesis, we first assessed the effects of HCA on iron

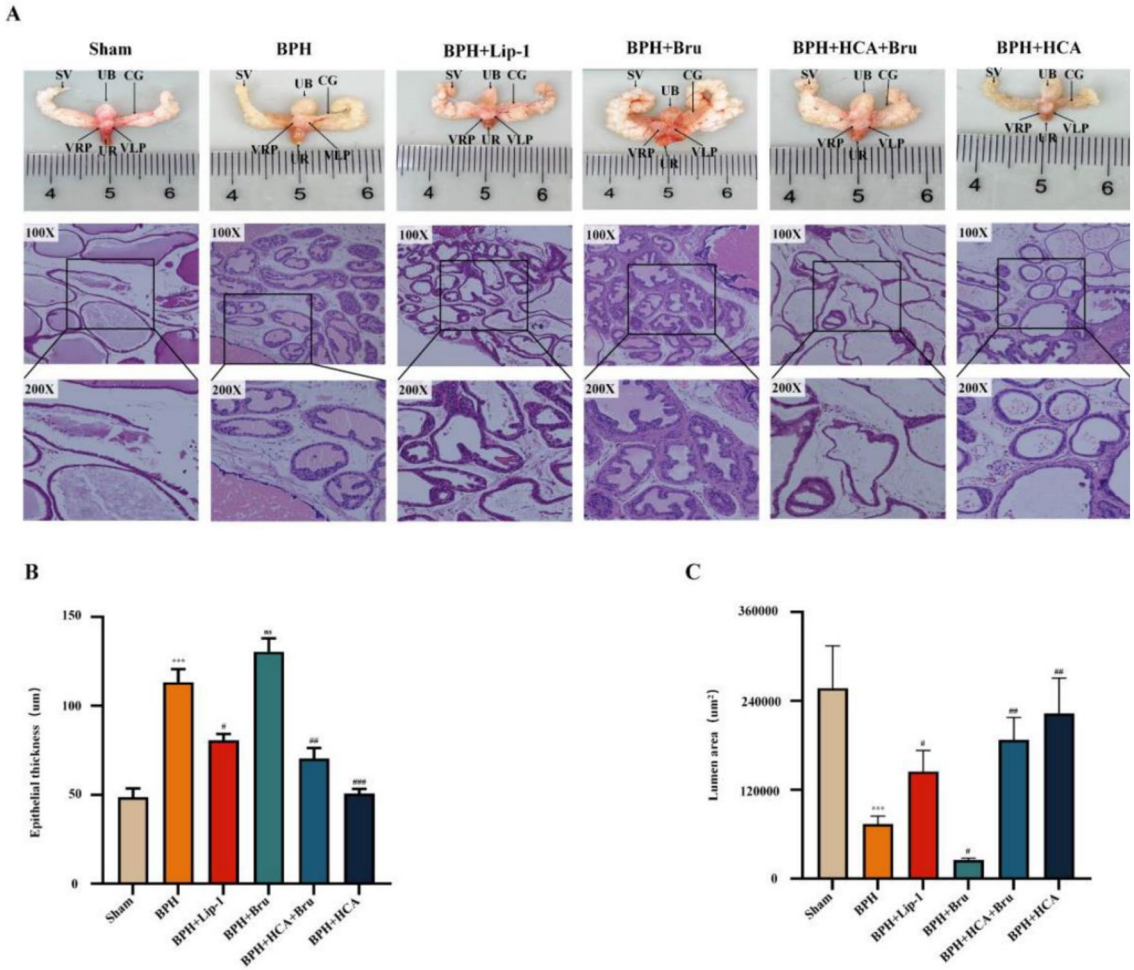

Fig. 3 illustrates the degree of prostatic hyperplasia in different groups. **A** Displays ex vivo images of the prostate along with HE staining images; **B** A statistical analysis of the thickness of prostatic epithelial cells; **C** A statistical analysis of the lumen area of prostatic epithelial cells. The figure labels the various structures: *SY* seminal vesicle, *CG* coagulating gland, *UB* bladder, *VRP* ventral right prostate, *VLP* ventral left prostate, and *UR* urethra. Data are presented as mean ± standard deviation (M ± SD).Comparisons with the Sham group indicate ***P < 0.001; comparisons with the BPH group indicate #P < 0.05, ##P < 0.01, and ###P < 0.001

levels and lipid peroxidation. Consistent with our expectations, after HCA treatment, levels of Fe^{2+} and MDA were significantly reduced compared to the BPH group, while GSH levels showed a notable increase (Fig. 4A–C). It is well known that glutathione (GSH)-dependent antioxidant enzyme GPX4 plays a critical role in inhibiting ferroptosis by reducing lipid peroxidation. Therefore, we examined the expression changes of GPX4 following HCA intervention. Our analysis indicated that HCA treatment significantly upregulated the expression of GPX4 protein compared to the BPH group (Fig. 4D, E). These findings suggest that HCA not only reduces the levels of lipid peroxidation products and iron but also enhances the expression of GPX4 and GSH. Together with the significant improvement in pathological hyperplasia of BPH observed with HCA, these results further confirm that HCA can inhibit ferroptosis.

Nrf2 is a transcription factor that regulates the expression of the GPX4 antioxidant response element and exerts its antioxidant function through nuclear translocation [40, 41]. Therefore, to further explore whether HCA inhibits ferroptosis through the activation of the Nrf2/GPX4 pathway, we conducted additional experiments. Subsequently, we intervened using the Nrf2 pathway inhibitor Brusatol (Bru). The expression levels of Nrf2 and its downstream target protein GPX4 were assessed using Western blotting. We found that under the intervention of Bru alone, the levels of MDA and Fe^{2+} were significantly elevated in the BPH + Bru group compared to the BPH group. The change in GSH levels was not significant. However, the expression of Nrf2 and GPX4 proteins was significantly suppressed. In contrast, with the intervention of HCA alone, the levels of MDA and Fe^{2+} were significantly reduced in the BPH + HCA group

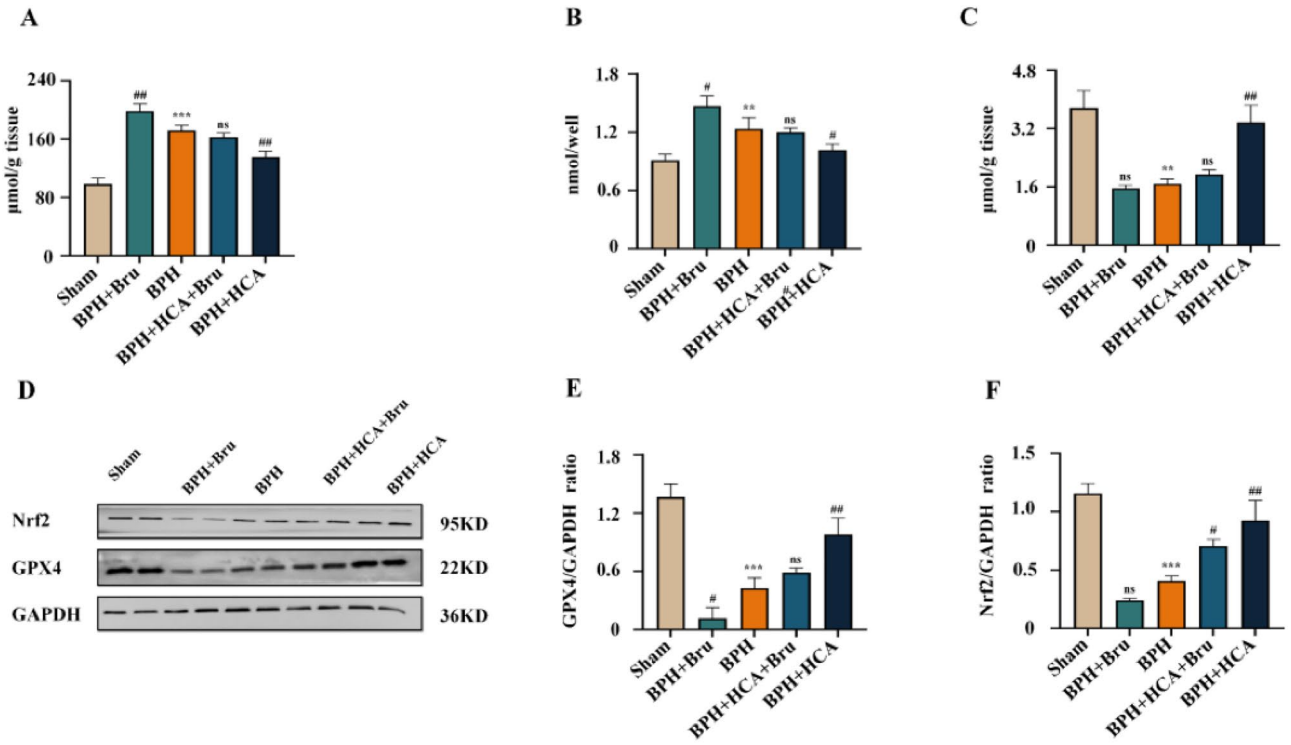

Fig. 4 HCA mitigates ferroptosis. **A**-**C** Levels of MDA, Fe^{2+}, and GSH in prostate homogenates of mice from different groups following HCA treatment. **D**-**F** Changes in the levels of GPX4 and Nrf2 proteins in the prostate of different groups following HCA treatment. Data are presented as mean ± standard deviation (M ± SD).Comparisons with the Sham group show **P < 0.01 and ***P < 0.001; comparisons with the BPH group show #P < 0.05 and ##P < 0.01

compared to the BPH group. Furthermore, GSH levels were significantly elevated, along with significant upregulation of Nrf2 and GPX4 protein expression. Following the combination treatment of Bru and HCA, the levels of MDA and Fe^{2+} were significantly decreased in the BPH + HCA + Bru group compared to the BPH + Bru group. The change in GSH levels was not significant. However, the expression of Nrf2 and GPX4 proteins was significantly increased in the BPH + HCA + Bru group compared to the BPH + Bru group (Fig. 4A–F). These results suggest that HCA may promote the nuclear translocation of Nrf2, activate the transcription of antioxidant genes, and thereby activate the Nrf2/GPX4 pathway to exert its protective effects against ferroptosis.

The effect of HCA on liver and kidney function-related parameters in a BPH animal model

Most drugs are primarily metabolized and excreted by the liver and kidneys. Their effects on liver and kidney function can provide direct insights into the safety of drug therapy. Therefore, the impact of drugs on liver and kidney function is often a critical prerequisite for the selection of therapeutic agents in clinical practice. To evaluate the effects of HCA, testosterone propionate, Liproxstatin-1, and Brusatol on liver and kidney function-related biochemical markers in our experiments, we selected commonly used clinical markers for assessing liver and kidney function impairment, including AST, ALT, SCR, and UR levels. Blood samples from each experimental group were subsequently analyzed. The results are shown in the figures. Compared to the Sham group, there were no significant elevations in AST, ALT, SCR, or UR levels in the BPH group (Fig. 5A–D). Similarly, the BPH + Lip-1, BPH + HCA, and BPH + Bru groups showed no significant increases in AST, ALT, SCR, or UR levels compared to the BPH group (Fig. 5E–H). When comparing the BPH + Bru and BPH + HCA groups to the BPH + HCA + Bru group, no significant changes were observed in AST, ALT, SCR, or UR levels (Fig. 5I–L). Furthermore, there were no significant changes in AST, ALT, SCR, or UR levels in the BPH + HCA group compared to the BPH + Bru group (Fig. 5M-P). To further assess the effects of HCA on liver and kidney injury, a one-year intervention study was conducted. The results showed no significant differences compared to the Sham and BPH groups (see Supplementary Fig. 1). These results indicate that testosterone propionate, HCA, Liproxstatin-1, and Brusatol have no significant effects on the liver and kidney function-related

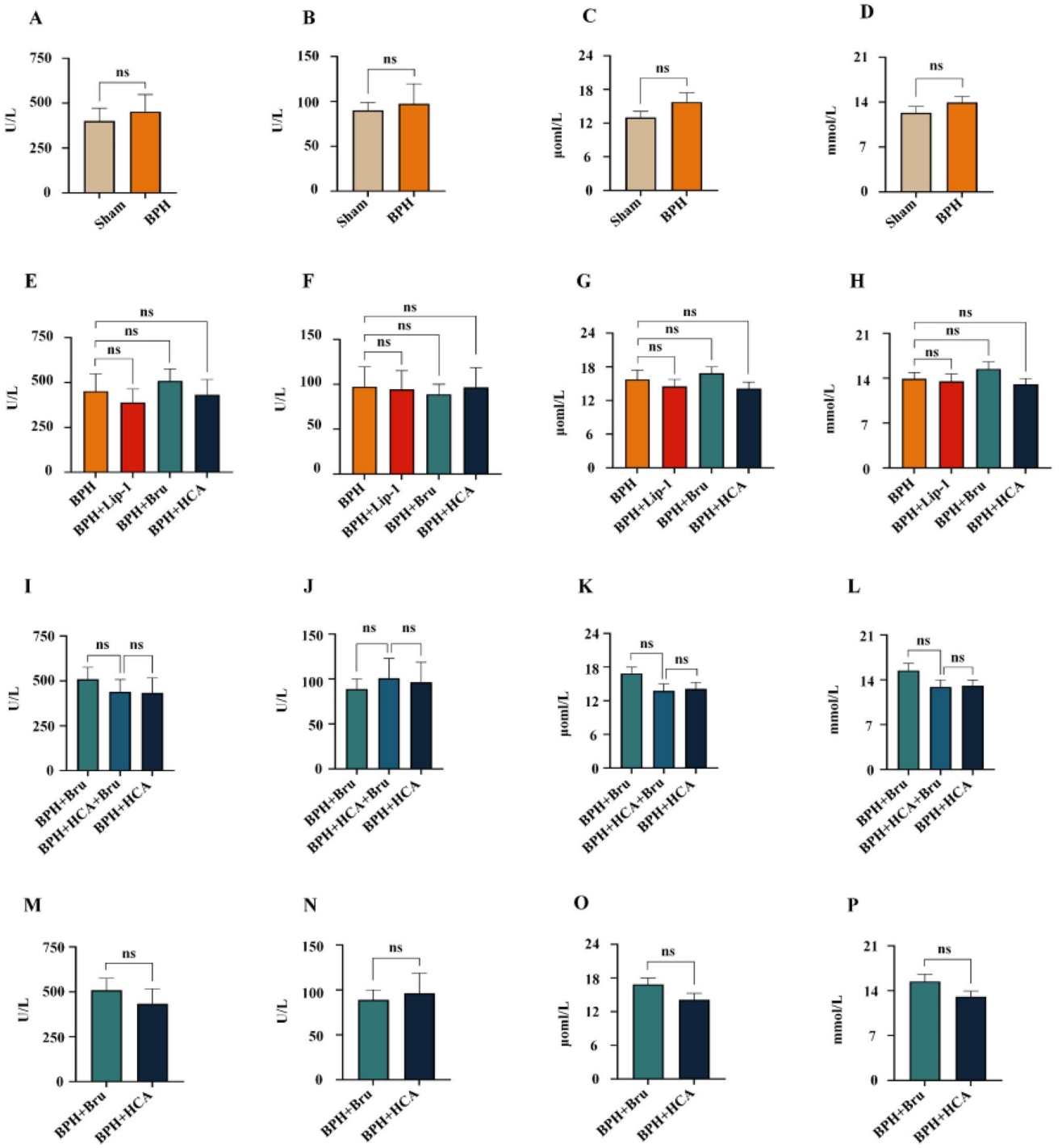

Fig. 5 The levels of AST (**A**, **E**, **I**, **M**), ALT (**B**, **F**, **J**, **N**), SCR (**C**, **G**, **K, O**), and UR (**D**, **H**, **L**, **P**) were assessed across different experimental groups. Comparisons with the Sham group (**A**, **B**, **C**, **D**) revealed no significant differences, with a p-value of ns $p > 0.05$. Similarly, there were no significant differences when compared to the BPH group (**E**, **F**, **G**, **H**), also with ns $p > 0.05$. Furthermore, comparisons with the BPH + HCA + Bru group (**I**, **J**, **K**, **L**) indicated no significant differences, maintaining a p-value of ns $p > 0.05$. Lastly, no significant differences were found in comparisons with the BPH + Bru group (**M**, **N**, **0**, **P**), with ns $p > 0.05$

markers (AST, ALT, SCR, and UR) in the BPH animal model.

Discussion

BPH is a prevalent health issue affecting middle-aged and older men worldwide, presenting a significant challenge to global public health. According to data compiled from various countries and regions by the Global Burden of Disease study, the global incidence of benign prostatic hyperplasia (BPH) increased from 51 million in 2000 to 94 million in 2019, indicating a rising burden of this disease over the years [42]. Studies indicate that BPH prevalence varies not only among different ethnicities—for example, African American and Hispanic men exhibit higher rates, while Asian men have relatively lower risks—but that Asian individuals are more susceptible to moderate to severe lower urinary tract symptoms (LUTS) associated with BPH compared to their European and American counterparts. Moreover, regional differences are pronounced, with the lowest prevalence of BPH observed in the central and southwestern populations, whereas the highest rates are found in the northwestern regions [43, 44]. These ethnic and regional disparities may be attributed to multiple factors, including genetic backgrounds, lifestyle habits, dietary cultures, and healthcare access [43]. Patients with BPH often experience LUTS and may also present with a range of comorbidities, posing significant threats to their quality of life. Based on clinical symptoms, BPH can be classified into three stages: storage symptoms, voiding symptoms, and post-voiding symptoms. Storage symptoms typically include increased urinary frequency, urgency, incontinence, and nocturia; during the voiding phase, patients may experience hesitancy, straining, and intermittency of urination; while post-voiding symptoms primarily manifest as a sensation of incomplete emptying and dribbling. The treatment goals for BPH are clear: the short-term objective is to alleviate LUTS, while the long-term focus is on slowing disease progression and preventing related complications. Currently, while pharmacological and surgical interventions are important for the treatment of BPH, comprehensive management strategies should not be overlooked. This includes interventions in patient lifestyle behaviors and dietary adjustments, such as encouraging regular exercise, optimizing urination habits, engaging in pelvic floor exercises, and avoiding high intake of caffeine and alcohol. To better understand the pathogenesis of BPH and explore effective treatment options, numerous scholars have analyzed clinical characteristics and conducted extensive experimental research leading to the development of various animal models of BPH, including testosterone induction, estrogen induction, high-fat diet induction, and transgenic methods [45–47]. Given that subcutaneous injection of testosterone propionate (TP) is commonly used to induce animal models of BPH, it serves as an effective method to confirm the etiology, pathophysiological evidence, and pharmacological data associated with BPH. This approach is characterized by high concordance with clinical diagnostic criteria, good reproducibility, and ease of model establishment, making it one of the most frequently utilized modeling techniques in contemporary research. Considering its advantages in model establishment simplicity and its close resemblance to clinical pathological diagnoses, this study adopts this method to induce a BPH mouse model. This model provides a crucial platform for subsequent research into the mechanisms of disease and the evaluation of therapeutic efficacy.

Ferroptosis, a newly discovered form of non-apoptotic programmed cell death, has garnered significant attention from the global scientific community since its introduction in 2012. Morphologically, ferroptosis differs significantly from apoptosis, necrosis, and autophagy, with four main characteristics: (1) Iron dependency: the process of ferroptosis requires the involvement of iron, which is the primary reason for its naming; (2) Disruption of redox homeostasis: prior to ferroptosis, an abnormal increase in intracellular reactive oxygen species (ROS) can be detected, accompanied by a significant reduction in reduced NADPH; (3) Distinct morphological changes in mitochondria: under transmission electron microscopy, notable mitochondrial boundary shrinkage, reduced volume, shape change from elongated rod-like to dot-like, and increased density of the double membrane are characteristic features of ferroptosis; (4) Regulatability: Ferroptosis can be reversed by lipophilic antioxidants (such as Fer-1 and Lip-1) or iron chelators, but is resistant to inhibitors of apoptosis (such as Z-VAD-FMK) or autophagy inhibitors (such as wortmannin) [17, 48]. Studies have indicated that multiple transcription factors are associated with the pathogenesis of ferroptosis [48], and many genes related to iron metabolism and ferroptosis are regulated by the transcription factor Nrf2, including transferrin (TF), transferrin receptor 1 (TfR1), and ferroportin (FPN1) [49, 50]. Additionally, this includes heme oxygenase 1 (HMOX1), glutathione (GSH), and glutathione peroxidase 4 (GPX4) [21, 51]. Normal cells can regulate membrane damage caused by lipid peroxides through antioxidant systems such as GPX4. When the antioxidant system becomes inactive, or in the presence of molecular oxygen and iron ions, the accumulation of lipid peroxides surpasses their regulatory capacity, leading to the occurrence of ferroptosis. GPX4 is an essential antioxidant enzyme for maintaining cellular redox homeostasis; it converts glutathione (GSH) into oxidized glutathione (GSSG) and reduces cellular lipid peroxides (PL-OOH) to their corresponding alcohols (PL-OH) [52]. Therefore, inhibition of GPX4 activity can lead to the accumulation of lipid peroxides, increasing

cellular sensitivity to ferroptosis, while upregulation of GPX4 expression can suppress ferroptosis. Research both domestically and internationally suggests that ferroptosis is closely related to the occurrence and development of benign prostatic hyperplasia (BPH) [29–31]. Our study shows that in a dihydrotestosterone-induced BPH model, significant changes in ferroptosis-related biochemical markers (such as Fe^{2+}, MDA, GSH, and GPX4 levels) were observed. Furthermore, transmission electron microscopy revealed morphological changes, such as reduced mitochondrial size and a significant decrease in cristae, further corroborating the significant increase of ferroptosis in the BPH model. Interestingly, after intervention with the lipophilic antioxidant Lip-1, the changes in ferroptosis-related markers were reversed, and HE staining results indicated significant improvement in tissue pathological damage, suggesting that inhibiting ferroptosis may help ameliorate BPH. In conclusion, we propose that ferroptosis plays a role in regulating BPH and may further exacerbate tissue hyperplastic damage, which is critically important for the occurrence and progression of BPH.

Previous studies have shown that HCA effectively inhibits the activity of ATP citrate lyase in cells, reducing fat synthesis [39]. Additionally, HCA plays a significant role in combating obesity by increasing serotonin release, which suppresses hunger [53, 54]. Furthermore, an increasing body of evidence suggests that HCA has potential anti-tumor, anti-inflammatory, and antioxidant properties. These findings provide a theoretical basis for the application of HCA in the treatment of other diseases, prompting us to further explore its therapeutic potential for benign prostatic hyperplasia (BPH). Thus, we aim to elucidate the therapeutic effects of HCA on BPH using murine models and to investigate the underlying mechanisms. Experimental results indicate that following HCA intervention, compared to the BPH group, the HE staining results revealed a significant reduction in epithelial cell thickness and a notable increase in gland lumen area, along with a reversal of changes in ferroptosis-related markers, suggesting that HCA may improve BPH by suppressing ferroptosis. Nrf2, as a key transcription factor in the antioxidant response, regulates the expression of GPX4. Upon administering the Nrf2 inhibitor Brusatol, we observed a marked decrease in the expression levels of Nrf2 and GPX4 in the BPH + BPH + Bru group compared to the BPH group. Concurrently, the levels of MDA and Fe2 + significantly increased, and HE staining indicated a notable reduction in the lumen area of epithelial cells. Following HCA treatment, compared to the BPH + BPH + Bru group, HCA significantly upregulated the expression of Nrf2 and GPX4, inhibiting the elevations of MDA and Fe2 + levels. HE staining results indicated a significant reduction in epithelial cell thickness and a substantial increase in lumen area, successfully reversing the effects of Brusatol. These findings indicate that the expression level of Nrf2 is directly related to sensitivity to ferroptosis, potentially due to enhanced antioxidant activity following increased Nrf2 expression, which in turn reduces sensitivity to ferroptosis [55, 56]. This phenomenon can be attributed to the dual role of Nrf2: on one hand, Nrf2 promotes the expression of GSH and GPX4, enhancing the function of the antioxidant system; on the other hand, Nrf2 facilitates the expression of FPN1 to sequester or export excess iron, thereby reducing intracellular iron accumulation and preventing the onset of ferroptosis [57, 58]. Although there is still controversy regarding the impact of HCA on liver and kidney injuries, our findings did not reveal any evidence of increased hepatotoxicity or nephrotoxicity within the concentration range used in our experiments, consistent with previous reports [59–61]. However, it is important to note that our evaluation of HCA's effects on liver and kidney function was limited to certain parameters, and we did not assess potential damage to other vital organs, such as the brain, lungs, heart, and gastrointestinal tract. Therefore, the results do not fully reflect the absolute safety of the drug, and further investigation into the systemic effects of HCA and its safety profile is warranted.

Although this study preliminarily validated that HCA improves pathological changes in BPH by activating the Nrf2/GPX4 pathway to suppress ferroptosis, several limitations remain. Firstly, this study only performed in vivo experiments; given the complexity of the in vivo environment, it remains unclear whether HCA further treats BPH through other mechanisms or pathways. Secondly, the chemical reagents used in the experiments (such as Liproxstatin-1 and Brusatol) may have off-target effects, which could potentially influence the experimental outcomes. Finally, in future research, we plan to complement our findings with in vitro experiments and utilize gene editing technologies (such as CRISPR/Cas9) to regulate specific genes or construct transgenic mouse models, allowing for a more in-depth verification of the role of ferroptosis in the pathogenesis of BPH. Additionally, we will explore other ferroptosis-related molecular pathways that HCA may be involved in and identify more potential therapeutic targets. These studies will provide a more comprehensive experimental basis for the application of HCA in the treatment of BPH.

Conclusion

In summary, this study demonstrates that ferroptosis is indeed involved in the pathogenesis of benign prostatic hyperplasia (BPH) in the testosterone propionate (TP)-induced model. This finding provides strong evidence for further exploration of the pathogenesis of BPH and reveals the potential value of inhibiting ferroptosis as a novel

therapeutic target for BPH. Moreover, this study is the first to elucidate the therapeutic efficacy and mechanisms of action of HCA in BPH, providing a theoretical basis for clinical treatment of BPH.

Supplementary Information The online version contains supplementary material available at https://doi.org/10.1007/s00345-025-05637-x.

Acknowledgements We sincerely thank the Yuxi City Science and Technology Program (Project No. YF2024060) for funding this research. We also express our gratitude to the Pathology Department and Laboratory Department of the Sixth Affiliated Hospital of Kunming Medical University (Yuxi People's Hospital) for their technical support, which enabled our study to proceed smoothly.

Author contributions Fachun Tong and Dayong Yang contributed to the manuscript writing and funding acquisition; Yongjie Tang, Tao Li, Mingyao Lu, and Liangsheng Wei contributed to data analysis and interpretation; Dayong Yang, Chengxi Zhai, Junyu Ren, and Jinran Bai carried out the experimental research; Fachun Tong, Dayong Yang, and Rongyao Luo edited the manuscript. All authors have read and agreed to the final manuscript.

Data availability No datasets were generated or analysed during the current study.

Declarations

Conflict of interest The authors declare no competing interests.

Ethical approval All animal experimental procedures were conducted in accordance with the "Guide for the Care and Use of Laboratory Animals" by the National Institutes of Health, following formal approval from the Animal Ethics Review Committee of Kunming Medical University. The ethics committee approval number for this study is kmmu20240132.

References

1. Lim KB (2017) Epidemiology of clinical benign prostatic hyperplasia. Asian J Urol 4(3):148–151. https://doi.org/10.1016/j.ajur.2017.06.004
2. Robert G, De La Taille A, Descazeaud A (2018) Epidemiology of benign prostatic hyperplasia. Prog Urol 28(15):803–812. https://doi.org/10.1016/j.purol.2018.08.005
3. Liu D, Li C, Li Y et al (2023) Benign prostatic hyperplasia burden comparison between China and United States based on the global burden of disease study 2019. World J Urol 41(12):3629–3634. https://doi.org/10.1007/s00345-023-04658-8
4. Tamalunas A, Sauckel C, Ciotkowska A et al (2021) Inhibition of human prostate stromal cell growth and smooth muscle contraction by thalidomide: a novel remedy in LUTS? Prostate 81(7):377–389. https://doi.org/10.1002/pros.24114
5. Lian L, Gj C (2023) Benign prostatic hyperplasia and lower urinary tract symptoms. Acm 13(03):4208–4214. https://doi.org/10.12677/acm.2023.133603
6. Joseph DB, Henry GH, Malewska A et al (2022) 5-Alpha reductase inhibitors induce a prostate luminal to club cell transition in human benign prostatic hyperplasia. J Pathol 256(4):427–441. https://doi.org/10.1002/path.5857
7. McPherson SJ, Ellem SJ, Simpson ER, Patchev V, Fritzemeier KH, Risbridger GP (2007) Essential role for estrogen receptor beta in stromal-epithelial regulation of prostatic hyperplasia. Endocrinology 148(2):566–574. https://doi.org/10.1210/en.2006-0906
8. Fiard G, Stavrinides V, Chambers ES et al (2021) Cellular senescence as a possible link between prostate diseases of the ageing male. Nat Rev Urol 18(10):597–610. https://doi.org/10.1038/s41585-021-00496-8
9. Vickman RE, Aaron-Brooks L, Zhang R et al (2022) TNF is a potential therapeutic target to suppress prostatic inflammation and hyperplasia in autoimmune disease. Nat Commun 13(1):2133–2140. https://doi.org/10.1038/s41467-022-29719-1
10. Udensi UK, Tchounwou PB (2016) Oxidative stress in prostate hyperplasia and carcinogenesis. J Exp Clin Cancer Res 35(1):139–146. https://doi.org/10.1186/s13046-016-0418-8
11. Suarez Arbelaez MC, Nackeeran S, Shah K et al (2023) Association between body mass index, metabolic syndrome and common urologic conditions: a cross-sectional study using a large multi-institutional database from the United States. Ann med 55(1):2197–2003. https://doi.org/10.1080/07853890.2023.2197293
12. Koudonas A, Anastasiadis A, Tsiakaras S et al (2023) Overview of current pharmacotherapeutic options in benign prostatic hyperplasia. Expert Opin Pharmaco 24(14):1609–1622. https://doi.org/10.1080/14656566.2023.2237406
13. Katsimperis S, Kapriniotis K, Manolitsis I et al (2024) Early investigational agents for the treatment of benign prostatic hyperplasia'. Expert Opin Inv Drug 33(4):359–370. https://doi.org/10.1080/13543784.2024.2326023
14. Kaplan SA, Chung DE, Lee RK, Scofield S, Te AE (2012) A 5-year retrospective analysis of 5α-reductase inhibitors in men with benign prostatic hyperplasia: finasteride has comparable urinary symptom efficacy and prostate volume reduction, but less sexual side effects and breast complications than dutasteride. Int J Clin Pract 66(11):1052–1055. https://doi.org/10.1111/j.1742-1241.2012.03010.x
15. Ganzer CA, Jacobs AR, Iqbal F (2015) Persistent sexual, emotional, and cognitive impairment post-finasteride: a survey of men reporting symptoms. Am j mens health 9(3):222–228. https://doi.org/10.1177/1557988314538445
16. Sugianto R, Tirtayasa P, Duarsa G (2022) A comprehensive review of medical therapy on benign prostatic hyperplasia. Sexologies 31(1):52–60. https://doi.org/10.1016/j.sexol.2021.07.002
17. Dixon SJ, Lemberg KM, Lamprecht MR et al (2012) Ferroptosis: an iron-dependent form of nonapoptotic cell death. Cell 149(5):1060–1072. https://doi.org/10.1016/j.cell.2012.03.042

18. Stockwell BR, Friedmann Angeli JP, Bayir H et al (2017) Ferroptosis: a regulated cell death nexus linking metabolism, redox biology, and disease. Cell 171(2):273–285. https://doi.org/10.1016/j.cell.2017.09.021
19. Ma Q (2013) Role of nrf2 in oxidative stress and toxicity. Annu Rev Pharmacol 53(16):401–426. https://doi.org/10.1146/annurev-pharmtox-011112-140320
20. Yang WS, SriRamaratnam R, Welsch ME et al (2014) Regulation of ferroptotic cancer cell death by GPX4. Cell 156(1–2):317–331. https://doi.org/10.1016/j.cell.2013.12.010
21. Dodson M, Castro-Portuguez R, Zhang DD (2019) NRF2 plays a critical role in mitigating lipid peroxidation and ferroptosis. Redox Biol 23(21):1011–1018. https://doi.org/10.1016/j.redox.2019.101107
22. Brigelius-Flohé R, Maiorino M (2013) Glutathione peroxidases. Biochim Biophys Acta 1830(5):3289–3303. https://doi.org/10.1016/j.bbagen.2012.11.020
23. Ge MH, Tian H, Mao L et al (2021) Zinc attenuates ferroptosis and promotes functional recovery in contusion spinal cord injury by activating Nrf2/GPX4 defense pathway. CNS Neurosci Ther 36(8):156–163. https://doi.org/10.1111/cns.13657
24. Lei G, Zhang Y, Koppula P et al (2020) The role of ferroptosis in ionizing radiation-induced cell death and tumor suppression. Cell res 30(2):146–162. https://doi.org/10.1038/s41422-019-0263-3
25. Jakaria M, Belaidi AA, Bush AI, Ayton S (2021) Ferroptosis as a mechanism of neurodegeneration in Alzheimer's disease. J Neurochem 159(5):804–825. https://doi.org/10.1111/jnc.15519
26. Wang ZL, Yuan L, Li W, Li JY (2022) Ferroptosis in Parkinson's disease: glia-neuron crosstalk. Trends Mol Med 28(4):258–269. https://doi.org/10.1016/j.molmed.2022.02.003
27. Ichihara G, Katsumata Y, Sugiura Y et al (2023) MRP1-dependent extracellular release of glutathione induces cardiomyocyte ferroptosis after ischemia-reperfusion. Circ res 133(10):861–876. https://doi.org/10.1161/CIRCRESAHA.123.323517
28. Tuo QZ, Liu Y, Xiang Z et al (2022) Thrombin induces ACSL4-dependent ferroptosis during cerebral ischemia/reperfusion. Signal Transduct Tar 7(1):51–59. https://doi.org/10.1038/s41392-022-00917-z
29. Li Y, Zhou Y, Liu D et al (2023) Glutathione peroxidase 3 induced mitochondria-mediated apoptosis via AMPK /ERK1/2 pathway and resisted autophagy-related ferroptosis via AMPK/mTOR pathway in hyperplastic prostate. J Transl Med 21(1):575–583. https://doi.org/10.1186/s12967-023-04432-9
30. Zhou L, Li Y, Li J et al (2024) Multi-omics analysis to identify CBR3-AS1-hsa-miR-145-5p-MAP3K5 pathway as a ferroptosis-related ceRNA network in benign prostatic hyperplasia. Genes Dis 11(5):1011–10149. https://doi.org/10.1016/j.gendis.2023.101184
31. Zhan M, Xu H, Yu G et al (2024) Androgen receptor deficiency-induced TUG1 in suppressing ferroptosis to promote benign prostatic hyperplasia through the miR-188-3p/GPX4 signal pathway. Redox Biol 75(13):1032–1039. https://doi.org/10.1016/j.redox.2024.103298
32. Ismail A, Mokhlis HA, Sharaky M et al (2022) Hydroxycitric acid reverses tamoxifen resistance through inhibition of ATP citrate lyase. Pathol Res Pract 240(24):1542–1548. https://doi.org/10.1016/j.prp.2022.154211
33. Goudarzvand M, Afraei S, Yaslianifard S et al (2016) Hydroxycitric acid ameliorates inflammation and oxidative stress in mouse models of multiple sclerosis. Neural regen res 11(10):1610–1616. https://doi.org/10.4103/1673-5374.193240
34. Dong J, Li W, Du X et al (2023) Garcinia cambogia water extract alleviates insulin resistance and hepatic lipid accumulation in mice fed a high-fat diet. Food Nutr Res 67(36):196–205. https://doi.org/10.29219/fnr.v67.8977
35. Lu ZL, Song CK, Zou SS et al (2023) Hydroxycitric acid alleviated lung ischemia-reperfusion injury by inhibiting oxidative stress and ferroptosis through the Hif-1α pathway. Curr Issues Mol Biol 45(12):9868–9886. https://doi.org/10.3390/cimb45120616
36. Nair AB, Jacob S (2016) A simple practice guide for dose conversion between animals and human. J Basic Clin Pharm 7(2):27–31. https://doi.org/10.4103/0976-0105.177703
37. Chuah LO, Yeap SK, Ho WY, Beh BK (2012) Alitheen NB (2012) In vitro and in vivo toxicity of garcinia or hydroxycitric acid: a review. Evid-Based Compl Alt 36:1979–1985. https://doi.org/10.1155/2012/197920
38. Li J, Cao F, Yin HL et al (2020) Ferroptosis: past, present and future. Cell Death Dis 11(2):88–98. https://doi.org/10.1038/s41419-020-2298-2
39. Jena BS, Jayaprakasha GK, Singh RP, Sakariah KK (2002) Chemistry and biochemistry of (-)-hydroxycitric acid from Garcinia. J Agr Food Chem 50(1):10–22. https://doi.org/10.1021/jf010753k
40. Shi J, Ma C, Zheng Z et al (2023) Low-dose antimony exposure promotes prostate cancer proliferation by inhibiting ferroptosis via activation of the Nrf2-SLC7A11-GPX4 pathway. Chemosphere 339(45):1397–1442. https://doi.org/10.1016/j.chemosphere.2023.139716
41. Han JH, Park MH, Myung CS (2021) Garcinia cambogia ameliorates non-alcoholic fatty liver disease by inhibiting oxidative stress-mediated steatosis and apoptosis through NRF2-ARE activation. Antioxidants (Basel) 10(8):59–65. https://doi.org/10.3390/antiox10081226
42. Awedew FA, Han H, Abbasi B, et al (2022) The global, regional, and national burden of benign prostatic hyperplasia in 204 countries and territories from 2000 to 2019: a systematic analysis for the global burden of disease study 2019. Lancet Healthy Longev 3(11):754–776. https://doi.org/10.1016/S2666-7568(22)00213-6
43. Kristal AR, Arnold KB, Schenk JM et al (2007) Race/ethnicity, obesity, health related behaviors and the risk of symptomatic benign prostatic hyperplasia: results from the prostate cancer prevention trial. J Urology 177(4):1395–1400. https://doi.org/10.1016/j.juro.2006.11.065
44. Xu XF, Liu GX, Guo YS et al (2021) Global, regional, and national incidence and year lived with disability for benign prostatic hyperplasia from 1990 to 2019. Am J Mens Health 15(4):155–161. https://doi.org/10.1177/15579883211036786
45. Hieble JP (2011) Animal models for benign prostatic hyperplasia. Handb Exp Pharmacol 42(22):69–79. https://doi.org/10.1007/978-3-642-16499-6_4
46. Zhang J, Zhang M, Tang J et al (2021) Animal models of benign prostatic hyperplasia. Prostate Cancer 24(1):49–57. https://doi.org/10.1038/s41391-020-00277-1
47. Mahapokai W, Van Sluijs FJ, Schalken JA (2000) Models for studying benign prostatic hyperplasia. Prostate Cancer 3(1):28–33. https://doi.org/10.1038/sj.pcan.4500391
48. Dai C, Chen X, Li J, Comish P, Kang R, Tang D (2020) Transcription factors in ferroptotic cell death. Cancer Gene Ther 27(9):645–656. https://doi.org/10.1038/s41417-020-0170-2
49. Yang X, Park SH, Chang HC et al (2017) Sirtuin 2 regulates cellular iron homeostasis via deacetylation of transcription factor NRF2. J Clin Invest 127(4):1505–1516. https://doi.org/10.1172/JCI88574
50. Kerins MJ, Ooi A (2018) The roles of NRF2 in modulating cellular iron homeostasis. Antioxid Redox Sign 29(17):1756–1773. https://doi.org/10.1089/ars.2017.7176
51. Liu J, Yang G, Zhang H (2023) Glyphosate-triggered hepatocyte ferroptosis via suppressing Nrf2/GSH/GPX4 axis exacerbates hepatotoxicity. Sci Total Environ 86(53):1608–1614. https://doi.org/10.1016/j.scitotenv.2022.160839
52. Seibt TM, Proneth B, Conrad M (2019) Role of GPX4 in ferroptosis and its pharmacological implication. Free Radical Bio Med

133(22):144–152. https://doi.org/10.1016/j.freeradbiomed.2018.09.014
53. Hayamizu K, Hirakawa H, Oikawa D et al (2003) Effect of Garcinia cambogia extract on serum leptin and insulin in mice. Fitoterapia 74(3):267–273. https://doi.org/10.1016/s0367-326x(03)00036-4
54. Semwal RB, Semwal DK, Vermaak I, Viljoen A (2015) A comprehensive scientific overview of Garcinia cambogia. Fitoterapia 102(62):134–148. https://doi.org/10.1016/j.fitote.2015.02.012
55. Sun X, Ou Z, Chen R et al (2016) Activation of the p62-Keap1-NRF2 pathway protects against ferroptosis in hepatocellular carcinoma cells. Hepatology 63(1):173–184. https://doi.org/10.1002/hep.28251
56. Dodson M, de la Vega MR, Cholanians AB, Schmidlin CJ, Chapman E, Zhang DD (2019) Modulating NRF2 in disease: timing is everything. Annu Rev Pharmacol 59(25):555–575. https://doi.org/10.1146/annurev-pharmtox-010818-021856
57. Zhang J, Zhang L, Yao G, Zhao H, Wu S (2023) NRF2 is essential for iron-overload stimulated osteoclast differentiation through regulation of redox and iron homeostasis. Cell biol toxicol 39(6):3305–3321. https://doi.org/10.1007/s10565-023-09834-5
58. Meng X, Zhao W, Yang R et al (2025) Lignans from *Schisandra chinensis* (Turcz) Baill ameliorates cognitive impairment in Alzheimer's disease and alleviates ferroptosis by activating the Nrf2/FPN1 signaling pathway and regulating iron levels. J ethnopharmacol 341(63):1193–1199. https://doi.org/10.1016/j.jep.2025.119335
59. Ishii Y, Kaneko I, Shen M et al (2003) Safety of Garcinia cambogia extract in healthy volunteers: high-dose administration study II. J Oleo Sci 52(12):663–671. https://doi.org/10.5650/jos.52.663
60. Hayamizu K, Tomi H, Kaneko I, Shen M, Soni MG, Yoshino G (2008) Effects of Garcinia cambogia extract on serum sex hormones in overweight subjects. Fitoterapia 79(4):255–261. https://doi.org/10.1016/j.fitote.2007.12.003
61. Hayamizu K, Ishii Y, Kaneko I et al (2002) No-observed-adverse-effect level (NOAEL) and sequential-high-doses administration study on Garcinia cambogia extract in humans. J oleo sci 51(5):365–369. https://doi.org/10.5650/jos.51.365